This document is the accepted manuscript version of the following article:
Pfingsten, O., Klein, J., Protesescu, L., Bodnarchuk, M. I., Kovalenko, M. V., & Bacher, G. (2018). Phonon interaction and phase transition in single formamidinium lead bromide quantum dots. Nano Letters, 18(7), 4440-4446. https://doi.org/10.1021/acs.nanolett.8b01523

Phonon Interaction and Phase Transition in Single Formamidinium Lead Bromide Quantum Dots

Oliver Pfingsten[1], Julian Klein[1], Loredana Protesescu[2,3], Maryna I. Bodnarchuk[2], Maksym V. Kovalenko[2,3] and Gerd Bacher[1]

1. Werkstoffe der Elektrotechnik and CENIDE, Universität Duisburg-Essen, Bismarckstraße 81, 47057 Duisburg, Germany.

2. Laboratory for Thin Films and Photovoltaics, Empa – Swiss Federal Laboratories for Materials Science and Technology, Überlandstrasse 129, CH-8600 Dübendorf, Switzerland

3. Institute of Inorganic Chemistry, Department of Chemistry and Applied Biosciences, ETH Zürich, Vladimir Prelog Weg 1, CH-8093 Zürich, Switzerland.

ABSTRACT

Formamidinium lead bromide ($FAPbBr_3$) quantum dots (QDs) are promising materials for light emitting applications in the visible spectral region because of their high photoluminescence (PL) quantum yield (QY) and the enhanced chemical stability as compared to, for instance, methylammonium based analogues. Towards practical harnessing of their compelling optical characteristics, the exciton recombination process - in particular the exciton-phonon interaction and the impact of crystal phase transition - has to be understood in detail. This is addressed in this contribution by PL studies on single colloidal $FAPbBr_3$ QDs. Polarization resolved PL measurements reveal a fine structure splitting of excitonic transitions due to the Rashba effect. Distinct phonon replica have been observed within energetic distances of 4.3 ± 0.5 meV, 8.6 ± 0.9 meV and 13.2 ± 1.1 meV from the zero phonon line, which we attribute to vibrational modes of the lead bromide lattice. Additional vibrational modes of 18.6 ± 0.3 meV and 38.8 ± 1.1 meV are found and related to liberation modes of the formamidinium (FA) cation. Temperature depended PL spectra reveal a line broadening of the emission caused by exciton phonon interaction as well an unusual energy shift which is attributed to a crystal phase transition within the single QD.

KEYWORDS

formamidinium lead bromide, single quantum dots, phonon interaction, fine structure, phase transition

MAIN TEXT

Lead halide perovskites [$APbX_3$, where A=Cs, FA (formamidinium) or MA (methylammonium); X=Cl, Br, I] have been shown to be a highly promising class of semiconductor materials for applications in solar-cells with power conversion efficiencies above 22%[1-4] or in light-emitting devices.[5-14] In the optoelectronic context methylammonium lead halides are the materials studied the most, although the environmental and thermodynamic instabilities of the organic methylammonium cation hamper eventual practical applications.[15-19] Higher chemical stabilities have been attained in perovskites with Cs^+ and FA cations in place of MA. $FAPbBr_3$ and $FAPbI_3$ are characterized by a cubic crystal structure at room temperature,[20-22] while $CsPbX_3$ exhibit an orthorhombic crystal structure at room temperature.[23-26]

$CsPbX_3$ and $FAPbX_3$ perovskites in form of ligand-stabilized colloidal nanocrystals, also known as quantum dots (QDs), exhibit bright emission spanning the whole visible spectral range with photoluminescence quantum yields (PL QYs) of up to 100% for $CsPbI_3$ QDs and narrow emission linewidth with full width half maximum (FWHM) of less than 100 meV (e.g. down to 18 nm in the green spectral range) as well as radiative lifetimes of 15 – 116 ns.[21,22,27-32] In spite of the rapid development in material preparation and prototype devices, the fundamental understanding of the optical properties in these colloidal nanocrystals (NCs) is still in progress. Optical spectroscopy revealed that the band-edge levels are 2-fold degenerate and biexcitons as well as charged excitons (trions) and Auger recombination can contribute to the recombination process.[33,34] Further experimental and computational investigations of the defect structure in $CsPbX_3$ reveal most of the defect states being located within the bands; this is known as a very high defect tolerance of these QDs.[35-38]

Beside these analyses of QD ensembles, measurements on single cesium lead halide QDs came up only recently. For $CsPbX_3$ QDs, photon antibunching was observed at room temperature demonstrating single-photon emission.[39,40] High resolution PL spectroscopy reveals a fine structure splitting of the emission lines, [41-43] which is caused by the Rashba effect and leads to two or three emission lines with energetic distances in the meV regime.[44] Besides, phonon replica which have been attributed to TO-phonons[41] and LO-phonons,[45] have been observed in $CsPbBr_3$ NCs.

Formamidinium lead halide ($FAPbX_3$) QDs are less investigated up to now. Single-photon emission has been observed in $FAPbBr_3$ single QDs just recently,[46] but nothing is known about exciton-phonon interaction or fine structure effects in $FAPbX_3$ QDs.

Here we present an analysis of fine structure splitting, exciton-phonon interactions and phase transition in single $FAPbBr_3$ QDs using temperature-dependent and polarization-resolved PL spectroscopy. Several phonon replicas are observed and attributed to diverse vibrational and liberation modes of the lead bromide lattice and the formamidinium (FA) cation, respectively. Exciton-phonon interaction is found to result in a temperature dependent broadening of the emission linewidth and clear signatures of a phase transition around 100 K are found in a single $FAPbBr_3$ QD.

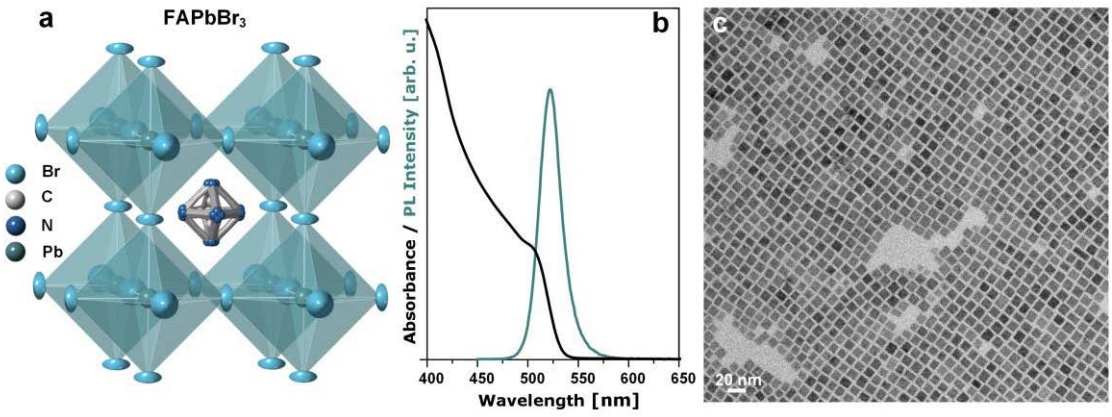

Figure 1. (a) Cubic crystal structure of $FAPbBr_3$ NCs at room temperature. FA cation is represented in a disordered state. (b) Room temperature absorbance and PL spectra of $FAPbBr_3$ NCs in toluene solution. (c) High-angle annular bright-field scanning electron microscopy image (HAABF-STEM) from an ensemble of $FAPbBr_3$ NCs.

Colloidal $FAPbBr_3$ QDs with nearly ideal cubic shape and an average size of 10 nm (see Figure 1), were prepared using a colloidal synthesis approach and are characterized by high PL QYs of typically 70 - 85 % and an emission in the green spectral range (peak wavelength of 530 nm) with a narrow FWHM of about 22 nm.[22] The PL peak energy is blue shifted as compared to bulk material (530 nm vs. 550 nm), indicating a regime of weak quantum confinement.[47]

For single QD spectroscopy, the QDs were embedded into poly(methyl methacrylate) (PMMA) and the mixture was spin coated onto a silicon substrate. Predefined positioning markers were used to enable a reproducible access to the same QD for various experimental conditions, like e.g. different temperatures. The measurements were carried out using a home-built micro-PL setup with a spectral resolution of 0.15 nm, covering a temperature range between

4 K and 350 K. Details of QD synthesis, sample preparation and experimental setup are described in the experimental section.

Measurements on a QD ensemble have been used to verify that the energetic position and linewidth of the emission do not change as a result of embedding into a PMMA matrix. An emission energy of 2.33 eV (532.2 nm) and a linewidth of 0.1 eV (22 nm) were still obtained. By gradually lowering the particle concentration, the emission spectra change from an unstructured broad emission spectra over multiple emission lines to narrow single emission lines with a width of 0.5 – 2 meV (see supporting information Figure S1). Single QD emission with similar linewidth is known from $CsPbX_3$ single QDs.[41,48]

For getting statistical relevant data, we have measured 32 individual QDs which were labeled #1 - #32 for individual identification later on. Scanning across the individual QDs by moving the laser spot does neither change the energy and linewidth nor the relative intensity between the different contributions of the single QD emission (fine structure split states, phonon replica, see below), indicating that single QDs are addressed. In Figure 2, polarization angle depended PL measurements of a typical single QD (labeled #32) are shown.

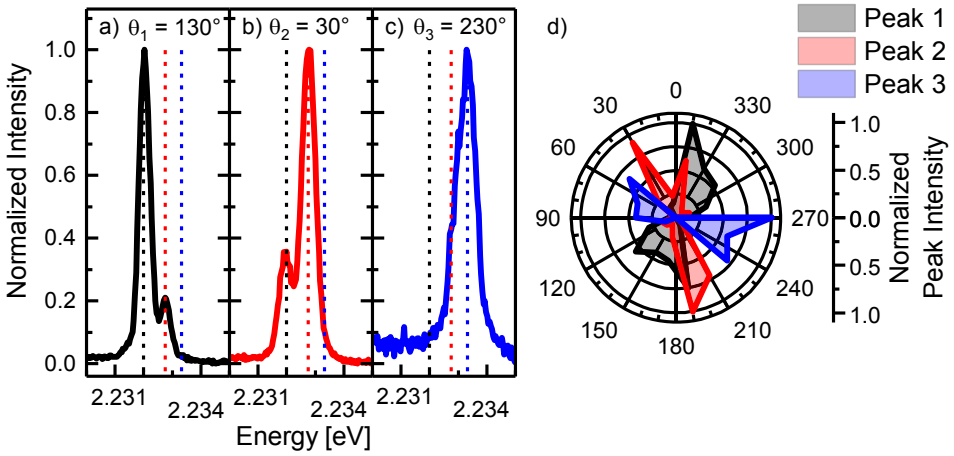

Figure 2. Normalized PL emission spectra from a single $FAPbBr_3$ QD excited with a power density of 130 W/cm² at a temperature of 4 K. The emission was detected with a linear polarizer in the detection pathway at polarization angles of (a) $\Theta_1 = 130°$, (b) $\Theta_2 = 30°$ and (c) $\Theta_3 = 230°$, respectively. The angles are given in relation to the laser polarization angle being at 0°. The polar plot of the normalized emission intensity from all 3 main emission peaks is shown in (d).

The normalized PL spectra depicted in Figure 2 (a – c) were detected with a linear polarizer in the detection pathway at polarization angles of $\Theta_1 = 130°$, $\Theta_2 = 30°$ and $\Theta_3 = 230°$, respectively. The angles are given in relation to the incident laser polarization angle being at 0°. We refer the individual emission lines to peak 1, peak 2 and peak 3 from lower to higher emission energies (see dotted lines). The energetic distance between two neighboring peaks is about 0.5 meV with a FWHM of 0.5 meV, which is limited by the setup used. Depending on the detection angle, the relative contribution of the three emission peaks changes. Because of the apparently polarized nature of the individual emission lines of the single QD we were able to extract the angle dependent intensity normalized to the maximum intensity per peak as shown in Figure 2 (d). As can be seen from the graph, peak 1 has its maximum intensity at an angle of $\Theta_{1,max} = 350°$, and peak 2 and 3 show maximum intensities at $\Theta_{2,max} = 190°$ and $\Theta_{3,max} = 270°$, respectively. Not all

of the 32 measured single QDs show 3 emission lines. Our statistical approach reveals that 10 out of 32 single QDs show 3 emission peaks, 7 only show two emission peaks and 15 are characterized by a single emission peak.

Similar observations have been reported earlier with $CsPbX_3$ single QDs and explained with an excitonic fine structure splitting in lead halide perovskites.[42,44,48] This splitting is mainly caused by two mechanisms. First, because of the strong spin-orbit coupling and the electron-hole exchange interaction the exciton splits into a dark J = 0 singlet and a bright J = 1 triplet state. Second, in semiconductors like lead halide perovskites with strong spin-orbit coupling and an inversion asymmetry a large Rashba effect occurs. According to Becker *et. al.* (see ref. 44), the Rashba effect splits the exciton triplet state into 3 bright states with transition dipoles oriented along the symmetry axis in case of orthorhombic symmetry - the symmetry of our QDs at low temperatures. Hereby, the breaking of the inversion symmetry required for a Rashba effect might arise from instabilities of the cation position[49] or from surface effects.[48] The emission from the individual sublevels seen in experiment is thus related to the orientation of the symmetry axes of each QD with respect to the direction of observation, i.e. a strong emission (no emission) is seen in case the dipoles are oriented perpendicular (parallel) to the observation axis. Thus, 1 - 3 emission lines should be visible, depending on the orientation of the individual nanocrystals with respect to the observation axis.[44] This is exactly what we observe in our $FAPbBr_3$ single QDs.

The angles of about 160° between the maximum intensities of peak 1 and 2 and about 80° between the maximum intensities of peak 2 and 3 are consistent with those observed in $CsPbX_3$ perovskite single NCs by M. A. Becker *et. al.* (see ref. 44). Also the energetic splitting of 0.5 - 2 meV for triple emissions and 1.5 - 2.2 meV for double emissions are comparable. Apparently, a similar excitonic fine structure like in $CsPbX_3$ is present in $FAPbBr_3$ single QDs having a

molecular, non-spherical cation instead of a single ion in the center of the lead bromide crystal cage. This indicates the general nature of this mechanism for lead halide perovskite QDs, in agreement with the predictions in ref. 44.

In addition to the fine structure splitting, satellite emission peaks have been detected at about 90% of the analyzed single QDs. These emissions cannot be referred to the fine structure splitting because the energetic distance from each other is much bigger, as can be seen in Figure 3.

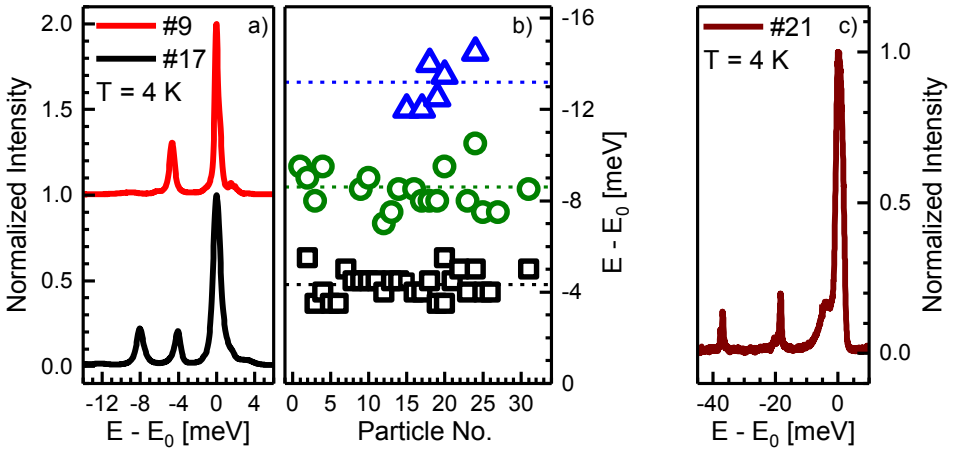

Figure 3. (a) Normalized emission spectra of two different single QDs (labelled #9 and #17) showing one or two satellite emission peaks at 4.5 meV (#9) and at 4.0 meV and 7.9 meV, respectively (#17), distance from the zero phonon line (ZPL). The energy axis is related to the ZPL emission energy E0. (b) Statistics over 32 different single QDs exhibiting one, two or three satellite peaks at an average distance of 4.3 meV, 8.6 meV and 13.2 meV from the ZPL. (c) Additional satellite peaks in the QD labelled #21 separated by about 18.3 meV and 37.2 meV from the ZPL. All data are obtained at T = 4 K.

In Figure 3 (a) normalized emission spectra of two characteristic single QDs (labelled #9 and #17) are shown. The ZPL emission energy E_0 is subtracted from the emission energy for simplified comparison. As one can see QD #9 shows one satellite peak shifted by 4.5 meV to lower energy as compared to the ZPL, whereas QD #17 has two satellite peaks at an energetic distance of 4.0 meV and 7.9 meV, respectively, from the ZPL. We did a statistical analysis of these emissions for all 32 QDs, which is summarized in Figure 3 b). In 27 out of 32 QDs the first satellite peak is observed at an average energetic distance of 4.3 ± 0.5 meV from the ZPL. The second satellite peak can be seen in 19 QDs with an average distance of 8.6 ± 0.9 meV. For 6 QDs, an additional emission peak with an average distance of 13.2 ± 1.1 meV from the ZPL is found.

As these emissions seem to be characterized by a well-defined energetic distance to the ZPL, we attribute them to phonon replica. Such kind of satellite peaks have not yet been observed in any organic lead halide perovskites, whereas similar emissions - however at distances of 3.7 meV and 6.3 meV, respectively, from the ZPL - have been found in $CsPbX_3$ perovskite single NCs and attributed to different TO phonon modes.[41] The fact that the intensity of the first order peaks raises linearly with higher excitation densities with the same slope as the main emission peak does (see supporting information Figure S2) is consistent with the assumption that these satellite peaks are related to phonon replica caused by exciton-phonon interaction during emission. The 3 replicas at energy E_1 (4.3 ± 0.5 meV), E_2 (8.6 ± 0.9 meV) and E_3 (13.2 ± 1.1 meV), respectively, clearly arise from different phonons as the energy splitting between the individual peaks within a single QD is not equidistant. This is confirmed by plotting the energy of the second phonon replica E_2 versus the energy E_1 of the first one for each individual QD. Hereby, it becomes obvious that for most of the QDs the energetic distance of the

second phonon replica E_2 to the ZPL is not twice the distance of the first replica E_1 to the ZPL (see supporting information Figure S3 (a)). This demonstrates that different phonons are involved. Also, according to the Huang-Rhys characteristics, the intensity of higher order phonon replica should be smaller than the one of the first replica, i.e. $I(E_3) < I(E_2) < I(E_1)$, which is in apparent contradiction to our data (see supporting information Figure S3 (b)). Thus, we attribute the phonon replica observed in our single QDs to be related to three different phonons.

This assignment is supported by comparing the determined phonon energies to Raman modes of lead halide perovskites discussed in literature. Lattice vibrations of lead halide perovskite are widely studied with Raman spectroscopy. Omer Yaffe *et. al.* analyzed $MAPbBr_3$ and $CsPbBr_3$ bulk single crystals and measured Raman modes with highest intensity at 29.8 cm^{-1}, 48 cm^{-1}, and 76.4 cm^{-1} corresponding to phonon energies of 3.7 meV, 6 meV and 9.5 meV for $CsPbBr_3$.[49] Similar values of 36.8 cm^{-1}, 47.4 cm^{-1} and 65.3 cm^{-1} (corresponding to 4.6 meV, 5.9 meV and 8.1 meV) are found for $MAPbBr_3$[49], i.e. the phonon energies of $CsPbBr_3$ and $MAPbBr_3$ are comparable.[50,51] These modes are attributed to the vibrations of the PbX_6 cage in $MAPbX_3$ and $CsPbX_3$ perovskites.[49,52-54] Detailed assignments of these modes were done by Dana M. Calistru *et. al.* analyzing a $CsPbCl_3$ bulk single crystal with Raman spectroscopy and comparing the data with theoretical considerations.[52] A double line with an energy around 4 meV was attributed to the TO_1 mode, a 9 meV resonance to the TO_2 mode and TO_3 as well as LO_1 modes are found to be located around 14.3 meV, while the modes around 6 meV are attributed to Cs^+ motions.[52] Taken this as a basis and comparing these numbers to the measured phonon replica energies in our $FAPbBr_3$ single QDs, we attribute the replica around 4.3 meV to the TO_1 mode and the one at 8.6 meV to the TO_2 mode. The satellite peak at a distance of around 13.2 meV from the ZPL is therefore assigned to either the TO_3 or the LO_1 mode or a combination of both.

Five of the measured single QDs show additional features at larger energetic distances from the ZPL as can be seen in Figure 3 (c). The emission of particle labelled #21 shows two extra peaks at a distance of 18.3 meV and 37.2 meV, respectively, from the ZPL. These two emissions are visible in five dots giving an average energy of 18.6 ± 0.3 meV and 38.8 ± 1.1 meV for these features, which are attributed to the first and second order contribution of another phonon mode. These energies are apparently much higher as expected for the vibrational modes of the PbBr6 cage. Considering Raman spectra discussed in literature, it becomes obvious that CsPbX3 does not show any Raman activity in this energetic region 52 but $MAPbX_3$ does.[50,55,56] Quarti et. al. calculated the energy for the methylammonium cation liberation modes of $MAPbX_3$ to be in the regions of 15 – 18 meV and 25 – 50 meV, respectively.[56] These calculated modes have also been observed in Raman spectra by other groups.[51,53] We thus conclude that the observed replica might be attributed to FA liberation modes; although values for their energy in lead halide perovskites have not been reported so far. However, we cannot exclude that these replica are related to the $PbBr_6$ cage octahedral mode, as discussed recently by Iaru *et al.* for $CsPbBr_3$.[45]

The lithographically defined marker system on the substrate allows us to track the emission of a single QD over a large temperature range. This gives experimental access to both phonon-induced linewidth broadening and temperature dependent bandgap shift in an isolated $FAPbBr_3$ QD. The temperature dependent PL spectra and emission FWHM as well as the temperature dependent energy shift are shown in Figure 4.

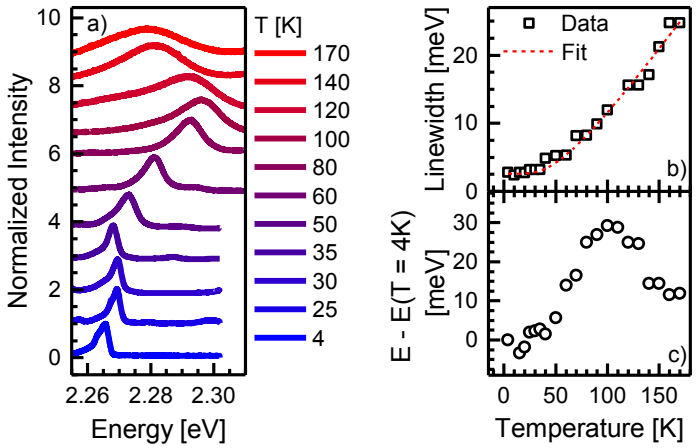

Figure 4. (a) Normalized emission spectra of a single $FAPbBr_3$ QD measured at different temperatures at an excitation power density of 130 W/cm². (b) Linewidth FWHM of the zero phonon line extracted from the PL spectra (symbols) and fitted according to equation (1). (c) Energy shift of the ZPL emission peak versus temperature in relation to the emission energy at T = 4 K for a single QD. The data correspond to the peak center energy of the spectra shown in (a).

The normalized emission spectra taken from a single QD at different temperatures are shown Figure 4 (a). The main emission peak shifts from 2.265 eV at 4 K to 2.298 eV at 120 K and then back to lower emission energies reaching 2.278 eV at 170 K. In addition, a distinct broadening of the emission line can be seen increasing from 2.6 meV at 4 K up to 24.7 meV at 170 K (see Figure 4 (b).

It is well known in QDs that the line broadening of excitonic emission with increasing temperature is caused by exciton-LO-phonon interactions[57-61] Rudin and Reinecke have shown that the linewidth broadening follows a Bose-Einstein statistics:[62]

$$\Gamma(T) = \Gamma_{inh} + \Gamma_{LA}T + \Gamma_{LO}\frac{1}{e^{\frac{E_{LO}}{k_bT}} - 1} \quad (1)$$

With Γ_{inh} as the inhomogeneous line broadening at 0 K, Γ_{LA} as the acoustic phonon (LA) coupling constant, E_{LO} as the LO-phonon energy and Γ_{LO} as the LO coupling constant. According to equation (1), LO phonon scattering can usually be considered as a main source of line broadening at elevated temperatures. The data fit very well with the formula (s. Figure 4 (b) red line) by setting E_{LO} = 13.2 meV, in very good agreement with the observed satellite peak which we related to the TO_3/LO_1 phonon replica in Figure 3. From the fitting values of Γ_{inh} = 2.6 meV for the inhomogeneous linewidth and Γ_{LO} = 31.8 meV for the LO-phonon coupling constant are obtained. The LA-coupling constant Γ_{LA} has to be much smaller than 0.1 meV to fit the data, so the contribution of LA phonon scattering can be neglected here.

Besides the linewidth broadening due to exciton-phonon interaction the single QD PL emission exhibits a quite unusual energy shift with temperature. The peak emission energy of the single QD was extracted from Figure 4 a) and is depicted versus temperature in Figure 4 c) in relation to the emission energy at T = 4 K. Emission energy shifts from 4 K to 100 K by about 30.6 meV to higher energies. Above 100 K, the emission energy successively drops reaching an energy red shift of about 18 meV at 170 K as compared to 100 K. A further increase of the temperature was impractical because of the decreasing signal / noise ratio.

Similar PL energy shifts with temperature have recently been observed by other groups on nanocrystal ensembles. Diroll *et. al.*[63] and Fang *et. al.*[64] studied $FAPbI_3$ nanocrystals exhibiting a blueshift up to 100 K followed by a red shift between 100 K and 150 K. This signature was related to a phase transition between the orthorhombic and the tetragonal phases.[63,64] This assignment is also supported by X-ray diffraction measurements on $FAPbBr_3$ bulk material

reported by Schueller *et. al.* revealing a cubic phase above 275 K, a tetragonal phase between 175 K and 275 K and an orthorhombic phase below 175 K.[65] Such phase transitions lead to a change of the materials bandgap[66]. Thus, the anomalous change of the emission energy observed in our single $FAPbBr_3$ QD in the temperature range between 100 K and 160 K is most likely attributed to a crystal phase transition between an orthorhombic phase at low temperatures and the tetragonal phase at elevated temperatures.

In summary, we have studied single $FAPbBr_3$ single QDs by polarization resolved and temperature dependent PL spectroscopy. A fine structure splitting with polarized emission peaks was found – in agreement to what is known for inorganic perovskite QDs – demonstrating the generality of this finding for colloidal perovskite QDs. Pronounced satellite peaks separated from the zero phonon line are identified and related to the TO_1, TO_2 and TO_3/LO_1 phonon modes with energies of 4.3 meV, 8.6 meV and 13.2 meV, respectively. Further replica at 18.6 ± 0.3 meV and 38.8 ± 1.1 meV could be attributed to liberation modes of the FA^+ cation within the center of the lead bromide cage. Temperature dependent PL spectroscopy has been used to identify the impact of exciton – phonon interaction on the homogeneous linewidth broadening and to visualize a phase transition from an orthorhombic to a tetragonal phase with increasing temperature. Such kind of phase transition has never been observed within any single QD up to now.

Methods.

Preparation of oleylammonium bromide (OAmBr). Ethanol (100 mL, Aldrich) and oleylamine (OAm, 12.5 mL, Acros Organics, 80-90 %) were mixed in a 250 mL flask. The reaction mixture was cooled in an ice-water bath and 8.56 mL HBr (48% aqueous solution, Aldrich) was added. The reaction mixture was left to react overnight under nitrogen flow. Then the solution was dried in a rotary evaporator and the obtained product was purified by rinsing multiple times with diethylether. The product (a white powder) was obtained after vacuum-drying at room temperature. OAmBr was stored in the glovebox.

Synthesis of $FAPbBr_3$ nanocrystals. In a 25 mL three-necked flask, lead (II) acetate trihydrate (76 mg, 0.2 mmol, Sigma-Aldrich) and formamidinium acetate (78 mg, 0.75 mmol, Sigma) were suspended in ODE (8 mL) and oleic acid (OAc, 2 mL, Sigma-Aldrich), heated to 50 °C and then dried under vacuum for 30 min. Subsequently, the reaction mixture was heated to 130 °C and, at this point, the mixture of 266 mg (0.8 mmol) of OAmBr in toluene (2 mL) was injected into the reaction flask. After another 1 min, the reaction mixture was cooled by a water-ice bath.

Isolation and purification of nanocrystals: 16 mL of methyl acetate (ABCR) were added to the crude solution followed by the centrifugation at 12.1 krpm for 5 min (Centrifuge: Eppendorf 5804) and the supernatant was discarded. The precipitate was dissolved in toluene (5 mL) and the solution was centrifuged again (3 krpm, 1 min). The supernatant, containing monodisperse nanocrystals, was retained for the DDAB-treatment, while the precipitated NCs were discarded.

DDAB-treatment of $FAPbBr_3$ nanocrystals. Before treatment, the $FAPbBr_3$ colloidal solution was washed again: 7 mL methyl acetate were added to 5 mL $FAPbBr_3$ colloidal solution, prepared as described above, followed by the centrifugation at 12.1 krpm for 3 min. The precipitate was redispersed in 10 mL toluene. 0.1 mL of OAc and 0.6 mL of DDAB (didodecyldimethylammonium bromide, 0.05 M in toluene) were added to 10 mL colloidal solution of $FAPbBr_3$ nanocrystals. The mixture was stirred for 1 h, followed by the precipitation with 16 mL of ethyl acetate and centrifuged at 12.1 krpm for 3 min. Precipitate was redispersed in 5 mL toluene and this solution was additionally filtered through a 0.45-□m PTFE-filter prior to optical measurements.

Preparation of a Single Quantum Dot. The synthesized QD dispersion in toluene with c = 5 mg/ml was diluted with pure toluene down to 0.005 mg/ml. 1 wt% PMMA (M_w = 20,000) was dissolved in toluene and then mixed 1:1 with the diluted QD dispersion. A silicon substrate was structured with periodically arranged gold markers (thickness 40 nm) using chromium or titanium (thickness 10 nm) as adhesive agent. Patterning has been done with electron beam lithography. The cross markers were added periodically with a distance of 15 µm between the markers. Each cross is 7x7 µm in size. The QD - PMMA mixture was then spin coated onto the pre-structured silicon substrate at 2000 rpm for 60 s.

Absorbance measurements. UV-VIS absorption spectra were collected using a Jasco V770 spectrometer operated in transmission mode.

Photoluminescence Spectroscopy. Fluoromax iHR 320 Horiba Jobin Yvon spectrofluorimeter equipped with a PMT detector was used to acquire steady-state PL spectra from colloidal solutions. The excitation wavelength was 400 nm, provided by a 450W Xenon lamp dispersed with a monochromator. Measured intensities were corrected to take into account the spectral response of the detector.

Transmission electron microscopy (TEM). Scanning TEM images were collected using a JEOL JEM-2200FS microscope operated at 200 kV.

Spatially Resolved Photoluminescence Spectroscopy. A home-built micro PL setup was used for the single quantum dot measurements. A 450 nm continues wave diode laser (Picoquant PDL-800D controller with PDL-450D laserhead) is focused by an optical microscope (magnification 63x, NA = 0.75) into a liquid helium cooled cryostat reaching a laser spot size of 1 µm. The temperature within the cryostat can be adjusted from 4 K up to 350 K. The setup is equipped with piezo-elements for motion control of the microscope objective, moving the focused beam onto the sample's surface. In the detection pathway the laser was cut off with an optical long-pass filter. For detecting the sample luminescence a monochromator (Horiba Scientific iHR-550) with an attached CCD device (Horiba Scientific CCD-3500) was used. A spectral resolution of 0.15 nm corresponding to an energetic resolution of about 0.5 meV in the considered wavelength region was achieved.

AUTHOR INFORMATION

Corresponding Authors

[1]E-Mail: gerd.bacher@uni-due.de

[2]E-Mail: mvkovalenko@ethz.ch

ACKNOWLEDGMENT

We would like to thank Bilge Bekdüz and Nicole Stracke for preparation of the patterned substrates. M.I.B. acknowledges financial support from the Swiss National Science Foundation (SNF Ambizione Energy grant, Grant No. PZENP2_154287). M.V.K. is grateful for financial support from the European Union through the FP7 (ERC Starting Grant NANOSOLID, GA No. 306733). M.I.B. and M.V.K. acknowledge Empa Electron Microscopy Center for the access to microscopes and technical assistance.

SUPPORTING INFORMATION

The following Figures are supplied as supporting

Figure S1. PL spectra of $FAPbBr_3$ QDs embedded in PMMA with different QD concentrations and measured at a temperature of 4 K with an excitation power density of 130 W/cm².

Figure S2. Intensity of the ZPL and the first order phonon replica E_1 versus excitation power density. The dashed lines have a slope of 1.

Figure S3. a) Energetic distance of the second phonon replica E_2 to the ZPL versus distance of the first replica E_1 to the ZPL. b) Intensity ratios $I(E_2) / I(E_3)$ versus $I(E_1) / I(E_2)$.

REFERENCES

(1) Yang, W. S.; Park, B. W.; Jung, E. H.; Jeon, N. J.; Kim, Y. C.; Lee, D. U.; Shin, S. S.; Seo, J.; Kim, E. K.; Noh, J. H.; Seok, S. Il. *Science.* **2017**, *356* (6345), 1376–1379.

(2) Yang, W. S.; Noh, J. H.; Jeon, N. J.; Kim, Y. C.; Ryu, S.; Seo, J.; Seok, S. I. *Science.* **2015**, *348* (6240), 1234–1237.

(3) Ahn, N.; Son, D. Y.; Jang, I. H.; Kang, S. M.; Choi, M.; Park, N. G. *J. Am. Chem. Soc.* **2015**, *137* (27), 8696–8699.

(4) National Center for Photovoltaics at the National Renewable Energy Laboratory, Research cell efficiency records, http://www.nrel.gov/ncpv/ (accessed 12 January 2018).

(5) Tan, Z.-K.; Moghaddam, R. S.; Lai, M. L.; Docampo, P.; Higler, R.; Deschler, F.; Price, M.; Sadhanala, A.; Pazos, L. M.; Credgington, D.; Hanusch, F.; Bein, T.; Snaith, H. J.; Friend, R. H. *Nat. Nanotechnol.* **2014**, *9* (9), 687–692.

(6) Yuan, M.; Quan, L. N.; Comin, R.; Walters, G.; Sabatini, R.; Voznyy, O.; Hoogland, S.; Zhao, Y.; Beauregard, E. M.; Kanjanaboos, P.; Lu, Z.; Kim, D. H.; Sargent, E. H. *Nat. Nanotechnol.* **2016**, *11* (10), 872-877.

(7) Meng, L.; Yao, E. P.; Hong, Z.; Chen, H.; Sun, P.; Yang, Z.; Li, G.; Yang, Y. *Adv. Mater.* **2017**, *29* (4), 1603826.

(8) Xiao, Z.; Kerner, R. A.; Zhao, L.; Tran, N. L.; Lee, K. M.; Koh, T. W.; Scholes, G. D.; Rand, B. P. *Nat. Photonics* **2017**, *11* (2), 108–115.

(9) Zhao, L.; Yeh, Y.-W.; Tran, N. L.; Wu, F.; Xiao, Z.; Kerner, R. A.; Lin, Y. L.; Scholes, G. D.; Yao, N.; Rand, B. P. *ACS Nano* **2017**, *11* (4), 3957–3964.

(10) Song, J.; Li, J.; Li, X.; Xu, L.; Dong, Y.; Zeng, H. *Adv. Mater.* **2015**, *27* (44), 7162–7167.

(11) Zhang, X.; Lin, H.; Huang, H.; Reckmeier, C.; Zhang, Y.; Choy, W. C. H.; Rogach, A. L. *Nano Lett.* **2016**, *16* (2), 1415–1420.

(12) Cho, H.; Kim, J. S.; Wolf, C.; Kim, Y.-H.; Yun, H. J.; Jeong, S.-H.; Sadhanala, A.; Venugopalan, V.; Choi, J. W.; Lee, C.-L.; Friend, R. H.; Lee, T.-W. *ACS Nano* **2018**, *12* (3), 2883–2892.

(13) Cho, H.; Kim, Y.-H.; Wolf, C.; Lee, H.-D.; Lee, T.-W. *Adv. Mater.* **2018**, 1704587.

(14) Kumar, S.; Jagielski, J.; Kallikounis, N.; Kim, Y. H.; Wolf, C.; Jenny, F.; Tian, T.; Hofer, C. J.; Chiu, Y. C.; Stark, W. J.; Lee, T. W.; Shih, C. J. *Nano Lett.* **2017**, *17* (9), 5277–5284.

(15) Niu, G.; Li, W.; Meng, F.; Wang, L.; Dong, H.; Qiu, Y. *J. Mater. Chem. A* **2014**, *2* (3), 705.

(16) Zhang, L.; Sit, P. H.-L. *J. Phys. Chem. C* **2015**, *119* (39), 22370–22378.

(17) Aristidou, N.; Sanchez-Molina, I.; Chotchuangchutchaval, T.; Brown, M.; Martinez, L.; Rath, T.; Haque, S. A. *Angew. Chemie - Int. Ed.* **2015**, *54* (28), 8208–8212.

(18) Ito, S. *APL Mater.* **2016**, *4* (9), 091504.

(19) Quitsch, W.-A.; DeQuilettes, D. W.; Pfingsten, O.; Schmitz, A.; Ognjanovic, S. M.; Jariwala, S.; Koch, S.; Winterer, M.; Ginger, D. S.; Bacher, G. *J. Phys. Chem. Lett.* **2018**, *9* (8), 2062–2069.

(20) Zhumekenov, A. A.; Saidaminov, M. I.; Haque, M. A.; Alarousu, E.; Sarmah, S. P.; Murali, B.; Dursun, I.; Miao, X.-H.; Abdelhady, A. L.; Wu, T.; Mohammed, O. F.; Bakr, O. M. *ACS Energy Lett.* **2016**, *1* (1), 32–37.

(21) Levchuk, I.; Osvet, A.; Tang, X.; Brandl, M.; Perea, J. D.; Hoegl, F.; Matt, G. J.; Hock, R.; Batentschuk, M.; Brabec, C. J. *Nano Lett.* **2017**, *17* (5), 2765–2770.

(22) Protesescu, L.; Yakunin, S.; Bodnarchuk, M. I.; Bertolotti, F.; Masciocchi, N.; Guagliardi, A.; Kovalenko, M. V. *J. Am. Chem. Soc.* **2016**, *138* (43), 14202–14205.

(23) Swarnkar, A.; Chulliyil, R.; Ravi, V. K.; Irfanullah, M.; Chowdhury, A.; Nag, A. *Angew. Chemie - Int. Ed.* **2015**, *54* (51), 15424–15428.

(24) Bertolotti, F.; Protesescu, L.; Kovalenko, M. V.; Yakunin, S.; Cervellino, A.; Billinge, S. J. L.; Terban, M. W.; Pedersen, J. S.; Masciocchi, N.; Guagliardi, A. *ACS Nano* **2017**, *11* (4), 3819–3831.

(25) Stoumpos, C. C.; Malliakas, C. D.; Peters, J. A.; Liu, Z.; Sebastian, M.; Im, J.; Chasapis, T. C.; Wibowo, A. C.; Chung, D. Y.; Freeman, A. J.; Wessels, B. W.; Kanatzidis, M. G. *Cryst. Growth Des.* **2013**, *13* (7), 2722–2727.

(26) Cottingham, P.; Brutchey, R. L. *Chem. Commun.* **2016**, *52* (30), 5246–5249.

(27) Kovalenko, M. V.; Protesescu, L.; Bodnarchuk, M. I. *Science.* **2017**, *358* (6364), 745–750.

(28) Akkerman, Q. A.; Rainò, G.; Kovalenko, M. V.; Manna, L. *Nat. Mater.* **2018**, *17*, 394–405.

(29) Protesescu, L.; Yakunin, S.; Bodnarchuk, M. I.; Krieg, F.; Caputo, R.; Hendon, C. H.; Yang, R. X.; Walsh, A.; Kovalenko, M. V. *Nano Lett.* **2015**, *15* (6), 3692–3696.

(30) Liu, F.; Zhang, Y.; Ding, C.; Kobayashi, S.; Izuishi, T.; Nakazawa, N.; Toyoda, T.; Ohta, T.; Hayase, S.; Minemoto, T.; Yoshino, K.; Dai, S.; Shen, Q. *ACS Nano* **2017**, *11* (10), 10373–10383.

(31) Koscher, B. A.; Swabeck, J. K.; Bronstein, N. D.; Alivisatos, A. P. *J. Am. Chem. Soc.* **2017**, *139* (19), 6566–6569.

(32) Dutta, A.; Dutta, S. K.; Das Adhikari, S.; Pradhan, N. *ACS Energy Lett.* **2018**, *3* (2), 329–334.

(33) Makarov, N. S.; Guo, S.; Isaienko, O.; Liu, W.; Robel, I.; Klimov, V. I. *Nano Lett.* **2016**, *16* (4), 2349–2362.

(34) Aneesh, J.; Swarnkar, A.; Kumar Ravi, V.; Sharma, R.; Nag, A.; Adarsh, K. V. *J. Phys. Chem. C* **2017**, *121* (8), 4734–4739.

(35) Huang, H.; Bodnarchuk, M. I.; Kershaw, S. V.; Kovalenko, M. V.; Rogach, A. L. *ACS Energy Lett.* **2017**, *2* (9), 2071–2083.

(36) Brandt, R. E.; Poindexter, J. R.; Gorai, P.; Kurchin, R. C.; Hoye, R. L. Z.; Nienhaus, L.; Wilson, M. W. B.; Polizzotti, J. A.; Sereika, R.; Žaltauskas, R.; Lee, L. C.; Macmanus-Driscoll, J. L.; Bawendi, M.; Stevanović, V.; Buonassisi, T. *Chem. Mater.* **2017**, *29* (11), 4667–4674.

(37) Ten Brinck, S.; Infante, I. *ACS Energy Lett.* **2016**, *1* (6), 1266–1272.

(38) Kang, J.; Wang, L. W. *J. Phys. Chem. Lett.* **2017**, *8* (2), 489–493.

(39) Park, Y. S.; Guo, S.; Makarov, N. S.; Klimov, V. I. *ACS Nano* **2015**, *9* (10), 10386–10393.

(40) Tang, X.; Hu, Z.; Chen, W.; Xing, X.; Zang, Z.; Hu, W.; Qiu, J.; Du, J.; Leng, Y.; Jiang, X.; Mai, L. *Nano Energy* **2016**, *28*, 462–468.

(41) Fu, M.; Tamarat, P.; Huang, H.; Even, J.; Rogach, A. L.; Lounis, B. *Nano Lett.* **2017**, *17* (5), 2895–2901.

(42) Rainoì, G.; Nedelcu, G.; Protesescu, L.; Bodnarchuk, M. I.; Kovalenko, M. V.; Mahrt, R. F.; Stöferle, T. *ACS Nano* **2016**, *10* (2), 2485–2490.

(43) Yin, C.; Chen, L.; Song, N.; Lv, Y.; Hu, F.; Sun, C.; Yu, W. W.; Zhang, C.; Wang, X.; Zhang, Y.; Xiao, M. *Phys. Rev. Lett.* **2017**, *119* (2), 026401.

(44) Becker, M. A.; Vaxenburg, R.; Nedelcu, G.; Sercel, P. C.; Shabaev, A.; Mehl, M. J.; Michopoulos, J. G.; Lambrakos, S. G.; Bernstein, N.; Lyons, J. L.; Stöferle, T.; Mahrt, R. F.; Kovalenko, M. V; Norris, D. J.; Rainò, G.; Efros, A. L. *Nature* **2018**, *553*, 189–193.

(45) Iaru, C. M.; Geuchies, J. J.; Koenraad, P. M.; Vanmaekelbergh, D.; Silov, A. Y. *ACS Nano* **2017**, *11* (11), 11024–11030.

(46) Yarita, N.; Tahara, H.; Saruyama, M.; Kawawaki, T.; Sato, R.; Teranishi, T.; Kanemitsu, Y. *J. Phys. Chem. Lett.* **2017**, 6041–6047.

(47) Hanusch, F. C.; Wiesenmayer, E.; Mankel, E.; Binek, A.; Angloher, P.; Fraunhofer, C.; Giesbrecht, N.; Feckl, J. M.; Jaegermann, W.; Johrendt, D.; Bein, T.; Docampo, P. *J.*

Phys. Chem. Lett. **2014**, *5* (16), 2791–2795.

(48) Isarov, M.; Tan, L. Z.; Bodnarchuk, M. I.; Kovalenko, M. V.; Rappe, A. M.; Lifshitz, E. *Nano Lett.* **2017**, *17* (8), 5020–5026.

(49) Yaffe, O.; Guo, Y.; Tan, L. Z.; Egger, D. A.; Hull, T.; Stoumpos, C. C.; Zheng, F.; Heinz, T. F.; Kronik, L.; Kanatzidis, M. G.; Owen, J. S.; Rappe, A. M.; Pimenta, M. A.; Brus, L. E. *Phys. Rev. Lett.* **2017**, *118* (13), 136001.

(50) Pistor, P.; Ruiz, A.; Cabot, A.; Izquierdo-Roca, V. *Sci. Rep.* **2016**, *6,* 35973.

(51) Park, M.; Kornienko, N.; Reyes-Lillo, S. E.; Lai, M.; Neaton, J. B.; Yang, P.; Mathies, R. A. *Nano Lett.* **2017**, *17* (7), 4151–4157.

(52) Calistru, D. M.; Mihut, L.; Lefrant, S.; Baltog, I. *J. Appl. Phys.* **1997**, *82* (11), 5391–5395.

(53) Park, B. W.; Jain, S. M.; Zhang, X.; Hagfeldt, A.; Boschloo, G.; Edvinsson, T. *ACS Nano* **2015**, *9* (2), 2088–2101.

(54) Ledinský, M.; Löper, P.; Niesen, B.; Holovský, J.; Moon, S. J.; Yum, J. H.; De Wolf, S.; Fejfar, A.; Ballif, C. *J. Phys. Chem. Lett.* **2015**, *6* (3), 401–406.

(55) Brivio, F.; Frost, J. M.; Skelton, J. M.; Jackson, A. J.; Weber, O. J.; Weller, M. T.; Go??i, A. R.; Leguy, A. M. A.; Barnes, P. R. F.; Walsh, A. *Phys. Rev. B* **2015**, *92* (14), 144308.

(56) Quarti, C.; Grancini, G.; Mosconi, E.; Bruno, P.; Ball, J. M.; Lee, M. M.; Snaith, H. J.; Petrozza, A.; Angelis, F. De. *J. Phys. Chem. Lett.* **2014**, *5* (2), 279–284.

(57) Heitz, R.; Mukhametzhanov, I.; Stier, O.; Madhukar, A.; Bimberg, D. *Phys. Rev. Lett.* **1999**, *83* (22), 4654–4657.

(58) Nirmal, M.; Norris, D. J.; Kuno, M.; Bawendi, M. G.; Efros, A. L.; Rosen, M. *Phys. Rev. Lett.* **1995**, *75* (20), 3728–3731.

(59) Bayer, M.; Forchel, A. *Phys. Rev. B* **2002**, *65* (4), 041308.

(60) Salvador, M. R.; Graham, M. W.; Scholes, G. D. *J. Chem. Phys.* **2006**, *125* (18), 184709.

(61) Arians, R.; Kümmell, T.; Bacher, G.; Gust, A.; Kruse, C.; Hommel, D. *Appl. Phys. Lett.* **2007**, *90* (10), 101114.

(62) Rudin, S.; Reinecke, T. L. *Phys. Rev. B* **1990**, *41* (5), 3017–3027.

(63) Diroll, B. T.; Guo, P.; Schaller, R. D. *Nano Lett.* **2018**, *18*, 846–852.

(64) Fang, H. H.; Protesescu, L.; Balazs, D. M.; Adjokatse, S.; Kovalenko, M. V.; Loi, M. A. *Small* **2017**, *13* (32), 1700673.

(65) Schueller, E. C.; Laurita, G.; Fabini, D. H.; Stoumpos, C. C.; Kanatzidis, M. G.; Seshadri, R. *Inorg. Chem.* **2018**, *57* (2), 695–701.

(66) Dar, M. I.; Jacopin, G.; Meloni, S.; Mattoni, A.; Arora, N.; Boziki, A.; Zakeeruddin, S. M.; Rothlisberger, U.; Grätzel, M. *Sci. Adv.* **2016**, *2* (10), e1601156–e1601156.